A photodecarboxylase from Micractinium conductrix active on medium and short-chain fatty acids

Ma, Yunjian; Zhong, Xuanru; Wu, Bin; Lan, Dongming; Zhang, Hao; Hollmann, Frank; Wang, Yonghua

DOI
10.1016/S1872-2067(22)64173-1

Publication date
2023

Document Version
Final published version

Published in
Chinese Journal of Catalysis

Chinese Journal of Catalysis 44 (2023) 160–170

available at www.sciencedirect.com

ScienceDirect

journal homepage: www.sciencedirect.com/journal/chinese-journal-of-catalysis

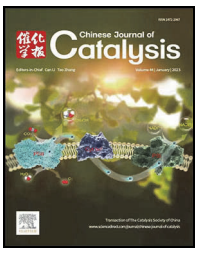

Article

A photodecarboxylase from *Micractinium conductrix* active on medium and short-chain fatty acids

Yunjian Ma [a,b], Xuanru Zhong [a], Bin Wu [c], Dongming Lan [a], Hao Zhang [a], Frank Hollmann [d,*], Yonghua Wang [a,e,*]

[a] *School of Food Science and Engineering, South China University of Technology, Guangzhou 510640, Guangdong, China*
[b] *Neher's Biophysics Laboratory for Innovative Drug Discovery, State Key Laboratory of Quality Research in Chinese Medicine, Macau University of Science and Technology, Taipa, Macau, China*
[c] *School of Bioscience and Bioengineering, South China University of Technology, Guangzhou 510006, Guangdong, China*
[d] *Department of Biotechnology, Delft University of Technology, Van der Maasweg 9, 2629HZ, Delft, The Netherlands*
[e] *Guangdong Youmei Institute of Intelligent Bio-manufacturing Co., Ltd, Foshan, Foshan 528200, Guangdong, China*

ARTICLE INFO

Article history:
Received 15 July 2022
Accepted 31 August 2022
Available online 10 December 2022

Keywords:
Photodecarboxylase
*Mc*FAP
Heterologous expression
Fatty acids
Hydrocarbon biofuel

ABSTRACT

Hydrocarbons are essential base chemicals as energy carriers and starting materials for chemical manufacture. So-called fatty acid photodecarboxylases (FAPs) represent interesting catalysts for the conversion of natural fatty acids into hydrocarbons thereby giving access to alkanes from renewable feedstock. Today, however, only few FAPs are known. In the current study we report a new FAP from the marine organism *Micractinium conductrix* (*Mc*FAP). In contrast to currently known FAPs *Mc*FAP exhibits high catalytic activity towards short and medium fatty acids. Recombinant expression and basic biochemical characterisation of this new member of the FAP family is reported.

1. Introduction

In recent years so-called fatty acid photodecarboxylases (FAPs) have gained considerable interest as catalysts for the conversion of fatty acids into the corresponding C1-shortened alkanes [1]. Especially compared to the existing chemical pendants FAPs enable this transformation under much milder reaction conditions and higher selectivity [2]. While chemical catalysts necessitate rather high reaction temperatures to operate well [3], FAPs only need activation by blue light (λ around 450 nm).

Since the description of the first FAP from *Chorella variabilis* (*Cv*FAP) by Beisson and coworkers in 2017 [4] this enzyme and its mutants have been investigated for a range of applications such as generation of fuels [5–16] or fine chemicals [17–19].

Today, however, FAP research has mainly focussed on *Cv*FAP. Other (putative) FAPs are principally known such as FAPs from *Chlamydomonas reinhardtii* (*Cr*FAP), *Ectocarpus siliculosus* (*Es*FAP), *Galdieria sulphuraria* (*Gs*FAP), *Nannochloropsis gaditana* (*Ng*FAP), but have not been studied in detail for their synthetic potential. *Cv*FAP, for example, has a preference for long-chain fatty acids, which to some extend can be ad-

* Corresponding author. E-mail: F.Hollmann@tudelft.nl (F. Hollmann), yonghw@scut.edu.cn (Y. Wang).
This work was supported by the National Outstanding Youth Science Foundation of China (31725022), Key Program of Natural Science Foundation of China (31930084), Project funded by China Postdoctoral Science Foundation (2020TQ0108), and Macau Young Scholars Program (AM2020024).
https://doi.org/10.1016/S1872-2067(22)64173-1

dressed by reaction [8] or enzyme engineering [10,15] but still represents a major limitation in substrate scope.

Overall, there is a clear need for more FAPs for preparative applications. We therefore mined publically available sequence databases identifying the putative FAP from *Micractinium conductrix* (*Mc*FAP), whose identification, expression and initial characterisation is reported in this contribution (Scheme 1).

2. Materials and methods

2.1. Chemical reagents and materials

All chemicals were purchased from Sigma-Aldrich, TCI, Oxoid Ltd (UK), Sanland Chemical Co., Ltd or Aladdin in the highest purity available and were used without further purification. *E. coli* BL21 (DE3) was used for the production of the biocatalyst and *E. coli* TOP10 was used for constructing *Mc*FAP and its mutants. Water was purified with a Millipore (Bedford, MA) Milli-Q water system.

2.2. Gas chromatographic analysis of the reactions

An Agilent 7890B GC system (Agilent Technologies, Palo Alto, CA, USA) was used together with a KB-FFAP GC column (Kromat Corporation, 4 Providence Court, Delran, NJ08075, USA. 30 m length × 0.25 mm I.D. × 0.25 μm film thickness). Method: injector temperature: 250 °C; split mode: 30:1; detector temperature: 280 °C.

GC oven temperature program: initial 110 °C, hold for 3.4 min, then from 110 to 190 °C at a ramp rate of 25 °C min^{-1}, hold for 2.1 min, from 190 to 230 °C at a ramp rate of 25 °C min^{-1}, then hold for 2 min, from 230 to 250 °C at a ramp rate of 30 °C min^{-1}, then hold for 12 min. Retention times are listed in Table S1.

2.3. Expression and purification of McFAP

Gene sequence derived from *Micractinium conductrix* (Genbank accession number: PSC67760.1) encoding the putative photodecarboxylase were synthesised by Sangon Biotech (Shanghai) Co., Ltd and cloned into the expression vector pET28a. The truncated mutant of *Mc*FAP 1–550 and *Mc*FAP 551–1146 amino acids deletion were constructed by PCR with primers pair listed in supporting information (Table S2) and the resulted gene sequence was cloned in the same vector using seamless cloning method. For expressing the *Mc*FAP wild type and its truncated mutant, the expression vector was transformed into the competent *E. coli* BL21 (DE3). The colony was firstly cultured in 5 mL LB medium (50 mg L^{-1} Kanamycin) and cultivated at 37 °C and 200 r min^{-1} for 12 h. 2 mL of this solution was used to inoculate a 100 mL LB medium (50 mg L^{-1} Kanamycin) in shake flasks. Upon reaching OD_{600} of ca. 0.8–1.1, IPTG was added in a final concentration of 0.5 mmol L^{-1} for another 21 h to induce the recombinant *Mc*FAP expression. Finally, the cells were pelleted by centrifugation. The resuspended cells (in buffer at 1:10 (*w*/*v*)) were disrupted by ultrasound treatment, followed by centrifugation (12000 r min^{-1} for 25 min) and the crude enzyme supernatant was collected.

*Mc*FAP was purified using a GE chromatography system. At first, the crude enzyme was load to a His Prep™ FF16/10 column pre-balanced by washing buffer A (50 mM Tris-HCl buffer, 300 mmol L^{-1} NaCl, 10 mmol L^{-1} imidazole, 5% (*w*/*v*) Glycerol, pH = 9.0) at a flow rate of 5 mL min^{-1}. After re-equilibrated with buffer A, the binding protein was eluted by elution buffer B (50 mM Tris-HCl buffer, 300 mmol L^{-1} NaCl, 500 mmol L^{-1} imidazole, 5% (*w*/*v*) glycerol, pH = 9.0) at a flow rate of 5 mL min^{-1}. After elution, the target protein was desalted by loading to the column HiPrep™ 26/10 with desalting buffer C (50 mmol L^{-1} Tris-HCl buffer, 150 mmol L^{-1} NaCl, 5% (*w*/*v*) glycerol, pH = 9.0) at a flow rate of 5 mL min^{-1}. The purified protein was stored at 4 °C.

2.4. Homologous modeling and molecular docking

The crystal structure for *Mc*FAP-S was unavailable, thus the homology model of *Mc*FAP-S was constructed using MODELLER. *Mc*FAP-S exhibits 78% amino acid identity to *Cv*FAP (PDB ID: 6ZH7) rendering the crystal structure of *Cv*FAP a suitable template to build the model of *Mc*FAP-S. Molecular operating environment (MOE) 2019.0102 was used to minimize the energy of the model and the result was used for the molecular docking study (using AutoDock).

2.5. Expression and purification of McFAP-S mutants

*Mc*FAP-S mutants were designed (Fig. S12) and the target genes were produced *via* PCR (primers used are shown in design is shown in Table S4). The monoclonal plasmids with correct sequencing results were extracted and transformed into the expression host *E.coli* BL21 (DE3) by heat shock transformation method for expression and purification. The purified mutant enzymes were obtained by nickel column affinity chromatography (Fig. S13).

2.6. Photoenzymatic reactions using recombinant McFAP

A representative reaction consisted of 500 μL wet *E. coli* cells containing *Mc*FAP (*Mc*FAP@*E. coli*) at 0.5 g mL^{-1} supplemented with 200 μL buffer (50 mmol L^{-1} Tris HCl, pH 9.0) and 300 μL 170 mmol L^{-1} fatty acid solution (dissolved in DMSO) in a 5 mL transparent reaction flask. This was placed in a self-made photocatalytic reaction device and reacted under 500 r min^{-1}, 30 °C and illuminated with blue light for 12 h. The

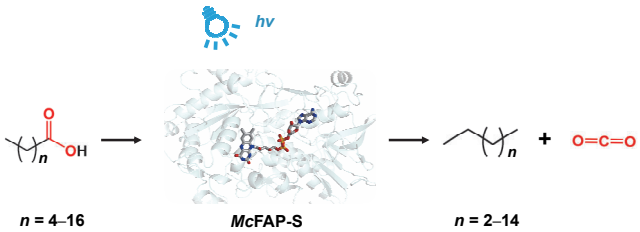

Scheme 1. The photodecarboxylase from Micractinium conductrix with a decarboxylation activity of medium and short-chain fatty acids.

homemade experimental setup is shown in Fig. S1. The blue LEDs (10 W) were purchased from Midea Co., Ltd. (Foshan, China). The distance between light source and reaction bottle was 2.5 cm. Afterwards the entire reaction mixtures were extracted with ethyl acetate (containing 25 mmol L^{-1} of 1-octanol as internal reference) in a 1:1 ratio (*v*/*v*). After centrifugation (11000 r min^{-1} for 4 min) the organic layer was analysed by gas chromatography.

2.7. Molecular dynamics simulations

Before the molecular dynamics simulations, the protonation states of the charged residues in the wt-*Mc*FAP-S and (Δ344–347) *Mc*FAP-S models were firstly determined by the H++ program and careful examination of their individual local hydrogen-bonding networks [20]. All His residues were determined as single protonated on the ε site. After the protonation determination, each prepared model was then neutralized by addition of Na^+ or Cl^- ions at the protein surface using the AmberTools package and finally, solvated in a rectangular water box with a 10 Å buffer distance between the solvent box wall and the nearest solute atoms. Meanwhile, the force field parameters of the FAD molecule was generated from the AMBER GAFF force field [21], and their partial atomic charges were obtained from the restrained electrostatic potential (RESP) charge at the HF/6-31G(d) level with the Gaussian 09 package [22]. All models were first minimized to relax the solvent and optimize the system. After several steps of minimization, each model was heated from 0 to 300 K gradually under the NVT ensemble for 100 ps, followed by another 150 ps of MD simulation under the NPT ensemble to relax the system density to about 1.0 g cm^{-3} with a target temperature of 300 K and a target pressure of 1.0 atm. Afterwards, with a target temperature of 300 K and a time step of 1.0 fs, 100 ns of NVT MD simulation under periodic boundary conditions was performed for each model to produce trajectories *via* the GPU accelerated pmemd program in the Amber 14 package [23]. During the MD process, the TIP3P model and Amber99SB force field were employed for the water molecules and proteins, respectively [24–27]. The SHAKE algorithm was applied to constrain all of the hydrogen-containing bonds with a tolerance of 10^{-5} [28]. The Langevin dynamics method was used to control the system temperature with a collision frequency of 1.0 ps^{-1} (ntt = 3, gamma_In = 1.0), and a cutoff of 12 Å was set for both van der Waals and electrostatic interactions [29].

3. Results and discussion

To identify promising photodecarboxylases candidates we used the amino acid sequence of *Cv*FAP as template and searched for homologues using the Blast module in NCBI. 490 gene sequences sharing amino acid identities between 35% and 80% with that of *Cv*FAP were found. Phylogenetic tree analysis of those sequences were conducted using MEGAN-X [30]. More than 50 phylogenetic trees were constructed using 5NCC-A as the root (Fig. 1). The sequence from *Micractinium conductrix* (Accession number: PSC67760.1) showed highest

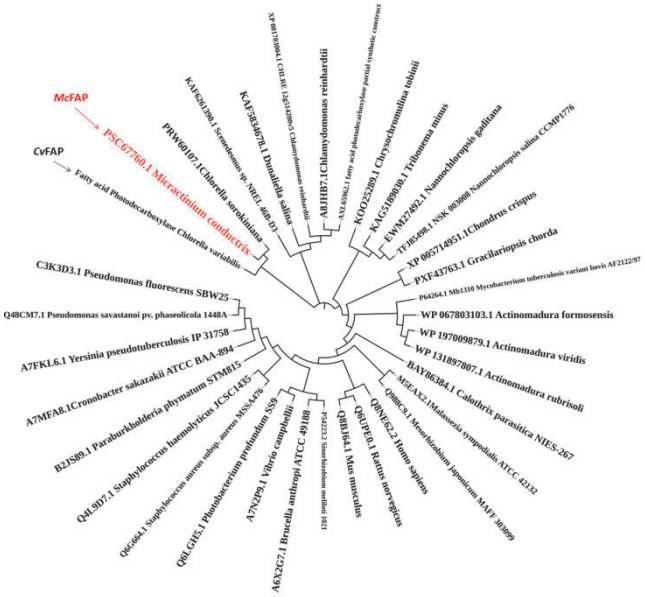

Fig. 1. Phylogenetic tree analysis of photodecarboxylases.

homology to *Cv*FAP (XP005842992.1) and contained the catalytically relevant amino acid residues in *Cv*FAP (Y466, N575, H572, Q486, T484, R451, I398, F469 and C432) [4,31]. Therefore, it implies that sequence PSC67760.1 may exhibit photodecarboxylase activity as *Cv*FAP.

Next, we functionally expressed *Mc*FAP in *Escherichia coli* and tested its photodecarboxylase activity on a range of fatty acids substrate (Fig. 2). Both, whole cells containing *Mc*FAP (*Mc*FAP@*E. coli*) and cell free extracts (CFE *Mc*FAP) showed the desired photodecarboxylase activity. Performing the experiments in the dark or using *E. coli* cell control did not result in detectable conversion of the starting material under otherwise

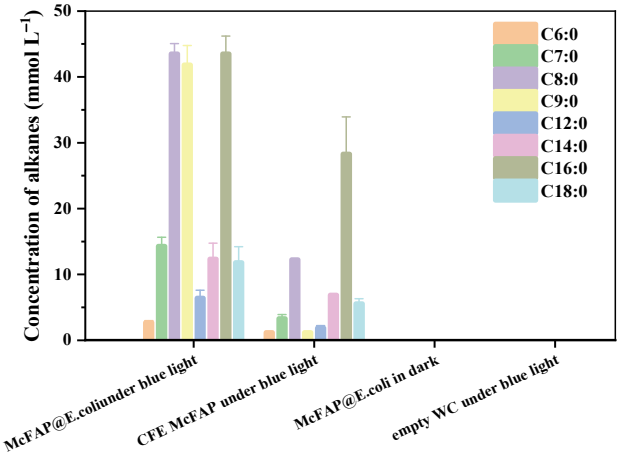

Fig. 2. *Mc*FAP decarboxylation validation reaction. Reaction conditions: 0.25 g mL^{-1} *Mc*FAP@*E. coli*, 20 mg mL^{-1} CFE *Mc*FAP or 0.25 g mL^{-1} empty whole cells, 50 mmol L^{-1} fatty acid substrate, 30% (*v*/*v*) DMSO, pH 9 buffer (50 mmol L^{-1} Tris-HCl) were mixed and under gentle magnetic stirring (500 r min^{-1}) at 30 °C in a total volume of 1 mL under the homemade photoenzymatic decarboxylation reaction setup (Fig. S1) for 12 h.

identical conditions.

Quite interestingly, *Mc*FAP, in contrast to *Cv*FAP exhibited significant activity towards shorter chain carboxylic acids such as octanoic and nonanoic acid. It is also interesting to note that the catalytic performance of *Mc*FAP confined in the *E. coli* cells was somewhat higher than within the cell free extracts. The latter observation may be due to a higher stability of the enzyme under these conditions.

According to the gene sequence, the molecular weight of *Mc*FAP was calculated as 117.8 kDa. However, SDS-PAGE electrophoresis analysis of the isolated sample after affinity chromatography manipulation showed that two proteins band with ca 62 and 69 kDa were found, respectively (Fig. 3). Mass spectroscopic analysis of the two protein bands (Fig. S2) suggested them belonged to C-terminal fragments (amino acids about 520 to 1146) of *Mc*FAP, consistent with the molecular mass determined via SDS-PAGE. The different lengths of N-terminal detachment lead to the appearance of two bands in SDS-PAGE. Apparently, the primary gene translation product underwent post-translational cleavage.

Sequence alignment of *Mc*FAP with *Cv*FAP (Fig. 4) revealed that especially the amino acids of 551–1146 in C-terminal regions show 78% sequence identities with that of *Cv*FAP by alignment analysis,while full length of *Mc*FAP gene and *Cv*FAP was only 41%. It was reported that the N-terminal region in *Cv*FAP does not contribute to the catalytic activity but rather ensures its localisation on the thylakoid membrane [32], we speculated that a similar organisation may be present in *Mc*FAP, i.e. that amino acids 1–540 may be irrelevant for its photodecarboxylase activity.

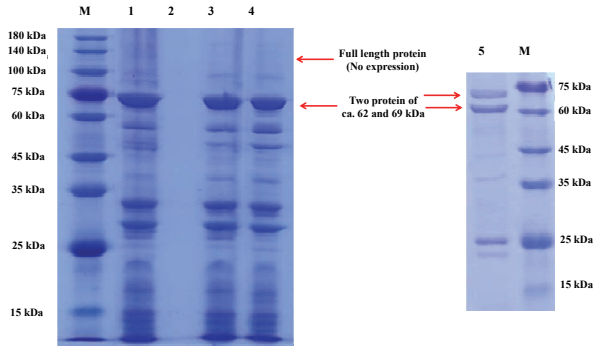

Fig. 3. SDS-PAGE analysis of the purified *Mc*FAP. Lane M: Protein Marker; Lane 1: whole cell protein; Lane 2: insoluble fraction; Lane 3: *Mc*FAP crude enzyme; Lane 4: purification passing sample; Lane 5: the protein sample eluted by buffer B.

Therefore, a truncated *Mc*FAP variant comprising amino acids 551–1146 was constructed (denoted as *Mc*FAP-S), and expressed in *E. coli*. As shown in Fig. 5, the truncated variant expressed significantly better than the wild-type enzyme and recombinant *Mc*FAP-S have been purified with a single band in the SDS-Page gel after affinity chromatography step (Fig. 5 and Table 1).

For the sake of completeness, we also constructed an N-terminal truncated variant (consisting of the original amino acids 1–540, denoted *Mc*FAP-N). The enzyme was heterologously expressed in *E. coli* and purified *via* Ni-affinity chromatography (Fig. S3). It was found that *Mc*FAP-N exhibited no catalytic activity towards any fatty acid substrates evaluated

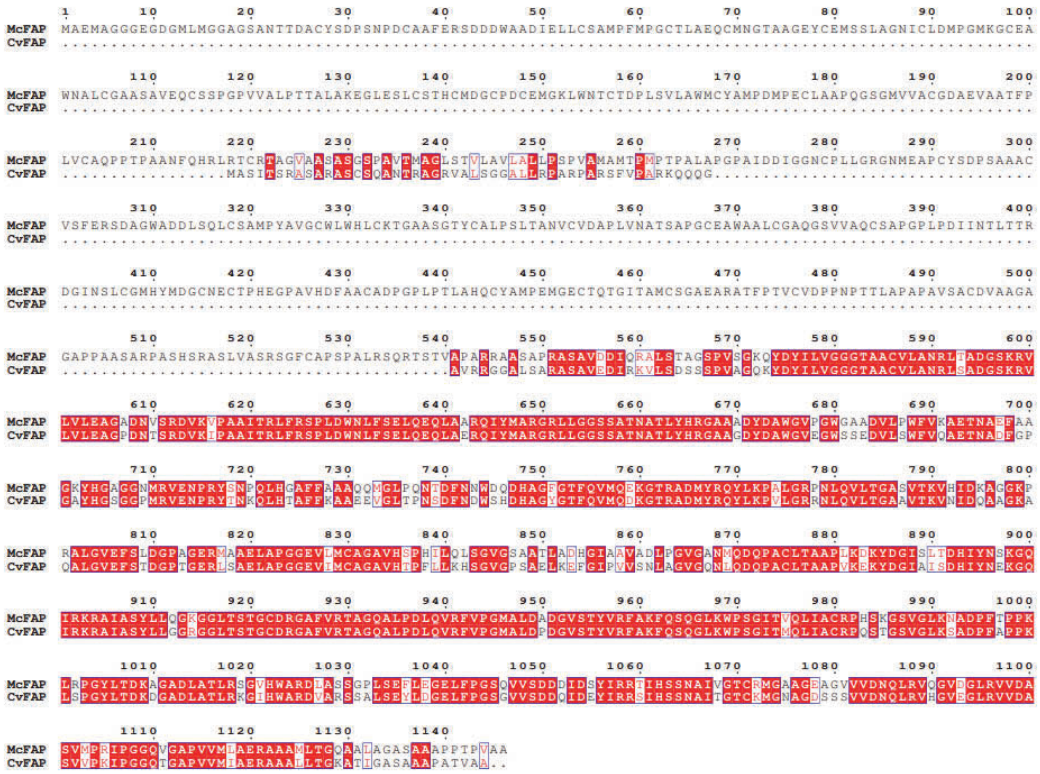

Fig. 4. Sequence alignment results of *Cv*FAP and *Mc*FAP.

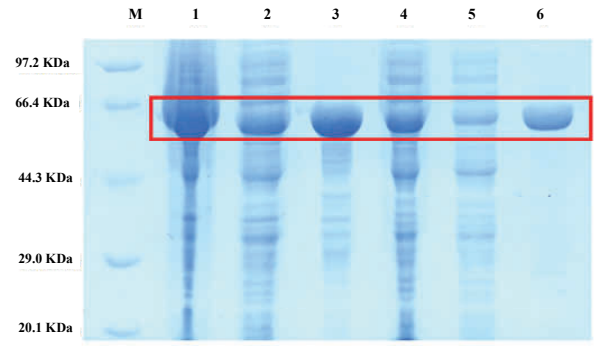

Fig. 5. SDS-PAGE analysis of McFAP-S. Lane M: protein marker; Lane 1: protein sample of total bacteria after lysis; Lane 2: total bacteria are broken and centrifuged to supernatant protein samples; Lane 3: total bacteria are broken and centrifuged to precipitate protein samples; Lane 4: McFAP-S crude enzyme protein sample; Lane 5: pass through the liquid protein sample when purified by nickel column; Lane 6: Purified McFAP-S sample eluted by buffer B.

Table 1
Purfication of *Mc*FAP-S.

Sample	Total protein (mg)	Total enzyme activity (U)	Specific enzyme activity (U mg^{-1})	Yield (%)
Crude enzyme solution	31800	2639	0.083	100
Affinity chromatography	836	334	0.399	13
After buffer change	595	159	0.268	6

(Table S3). But deleting the N-terminus of *Mc*FAP had no change the substrate specificity (Fig. 6).

We next performed a basic biochemical characterisation of *Mc*FAP-S evaluating the effect of polar organic solvents (Fig. S4(a)) and metal ions (Fig. S4(b)) on the activity of the enzyme. Methanol or DMSO had no apparent influence on the activity of

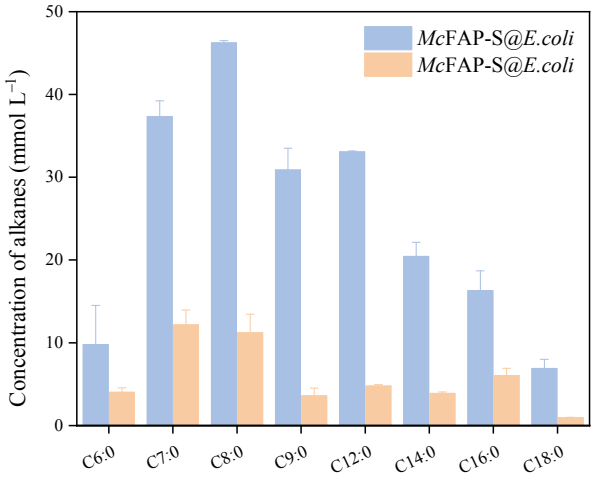

Fig. 6. Comparison of efficiency of *Mc*FAP@*E. coli* and *Mc*FAP-S@*E. coli* catalyzing decarboxylation of different chain length fatty acids. Reaction conditions: 0.25 g mL^{-1} *Mc*FAP-S@*E.coli* or *Mc*FAP@*E.coli*, 50 mmol L^{-1} fatty acid substrate, 30% (*v*/*v*) DMSO, pH = 9 buffer (50 mmol L^{-1} Tris-HCl) were mixed and under gentle magnetic stirring (500 r min^{-1}) at 30 °C in a total volume of 1 mL under the homemade photoenzymatic decarboxylation reaction setup (Fig. S1) for 1 h.

*Mc*FAP-S when incubated in the concentration of 30% (*v*/*v*), while ethanol or acetonitrile significantly decreased the catalytic activity of *Mc*FAP-S at the same concentration.

The influence of the reaction temperature on the activity and stability of *Mc*FAP-S is shown in Figs. 7(a), (b). *Mc*FAP-S showed highest product formation rates at 40 °C. Likewise, preincubating the enzyme (in the dark) at temperatures below 40 °C for 6 h did not result in a significant decrease of the enzyme activity. The half life time of *Mc*FAP-S at 50 °C was about 2 h. When stored at 4 °C in the dark, the enzyme can maintain more than 70% of its initial activity after 10 d (Fig. S5).

*Mc*FAP-S exhibited its maximal catalytic activity in slightly alkaline media between pH 8 and 9 (Figs. 7 (c), (d)). *Mc*FAP-S was stable in buffer with various pH value with residual activity higher than 50% after 5 h incubation (Fig. 7(d)).

Previous studies have shown that the photodecarboxylase *Cv*FAP is prone to photocatalytic inactivation [7,13]. To investigate whether *Mc*FAP suffers from similar limitations, the effect of external illumination on the stability of *Mc*FAP-S was measured (Fig. 8(a)). Very similar to *Cv*FAP, also *Mc*FAP was readily inactivated by blue light whereas wavelengths not overlapping with the flavin absorption spectrum (such as red light) hardly influenced the stability of the enzyme. The photoinactivation reaction could somewhat be alleviated in the presence of *n*-octanoic acid.

We therefore assume that the hypothesis of 'keeping the FAP busy' also applies to *Mc*FAP [7]. In other words, in the absence of a convertible fatty acid starting material photoexcited flavin within the enzyme active site undergoes photobleaching and/or oxidises catalytically relevant amino acids within the active site. Therefore, ensuing a maximal saturation of the enzyme active site with fatty acids alleviates photoinactivation. Next to octanoic acid also lauric acid and hexanoic acid exhibited a protective effect (Fig. 8(b)).

Next, we investigated the influence of catalyst- and starting material concentration on the rate of the photoenzymatic decarboxylation reaction (Fig. 9). Increasing the enzyme concentration up to 25 μmol L^{-1} resulted in a linear increase of the product formation rate. The average turnover frequency of the enzyme was 10 min^{-1} corresponding to a specific activity (A_{spec}) of 0.16 U mg^{-1}, comparable to the specific activity of *Cv*FAP under similar conditions. The catalytic activity was not influenced by varying the substrate concentration between 10 and 50 mmol L^{-1} indicating that the K_M value for *n*-octanoic acid is significantly below 5 mmol L^{-1}, though further studies will be needed to determine this value precisely. Similar observations were made using palmitic acid as starting material (Fig. S6 and Fig. S7).

An exemplary time course of the *Mc*FAP-catalysed decarboxylation of oxtanoic acid is shown in Fig. 9(b). Using, 60 μmol L^{-1} of the enzyme, 20 mmol L^{-1} of octanoic acid were fully converted (> 95% conversion) within 30 min.

Overall, *Mc*FAP-S exhibited similar biochemical properties as *Cv*FAP with the notable exception of carboxylic acids chain length preference. To obtain further insights into the molecular origins of this difference in substrate spectrum we compared the three-dimensional structures of both enzymes (using the published crystal structure for *Cv*FAP and a homology model of

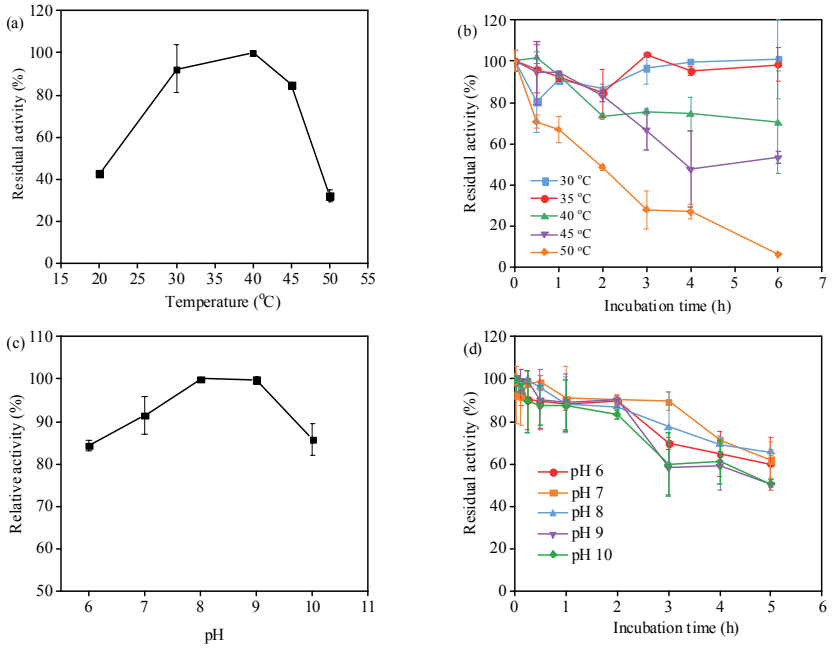

Fig. 7. Effect of temperature on *Mc*FAP-S activity (a), stability (b) and effect of pH on *Mc*FAP-S activity (c), stability (d). Reaction conditions: (a) Enzyme activity detection system: 20 μmol L^{-1} *Mc*FAP-S, 20 mmol L^{-1} *n*-octanoic acid, 15% (*v*/*v*) DMSO, 50 mmol L^{-1} Tris-HCl pH = 9 of 1 mL total system in a glass vials, 30 min, 500 r min^{-1}, under the homemade photoenzymatic decarboxylation reaction setup (Fig. S1). (b) Enzyme activity detection system: 20 μmol L^{-1} *Mc*FAP-S, 20 mmol L^{-1} *n*-octanoic acid, 15% (*v*/*v*) DMSO, 50 mmol L^{-1} Tris-HCl pH = 9 of 1mL total system in a glass vials, 500 r min^{-1}, under the homemade photoenzymatic decarboxylation reaction setup (Fig. S1). (c) For determination of pH optimum, the *Mc*FAP activity was measured at 30 °C using the following buffers: citrate-phosphate pH = 5 and 6, phosphate pH = 7, pyrophosphate pH = 8, Tris-HCl pH = 9 and 10 each at 50 mmol L^{-1} concentration. Enzyme activity detection system: 20 μmol L^{-1} McFAP-S, 20 mmol L^{-1} *n*-octanoic acid, 15% (*v*/*v*) DMSO, 50 mmol L^{-1} Tris-HCl pH = 9.0 of 1 mL total system in a glass vials, 30 min, 30 °C, 500 r min^{-1}, under the homemade photoenzymatic decarboxylation reaction setup (Fig. S1). (d) *Mc*FAP-S pure enzyme solution and gradient pH buffer (pH = 6, 7, 8, 9, 10) were taken respectively and incubated for a certain time (0, 0.04, 0.13, 0.25, 0.5, 1, 2, 3, 4 and 5 d) under the condition of avoiding light at 4 °C. Enzyme activity detection system: 20 μmol L^{-1} *Mc*FAP-S, 20 m mol L^{-1} *n*-octanoic acid, 15% (*v*/*v*) DMSO, 50 mmol L^{-1} Tris-HCl pH 9 of 1mL total system in a glass vials, 30 °C, 500 r min^{-1}, under the homemade photoenzymatic decarboxylation reaction setup (Fig. S1).

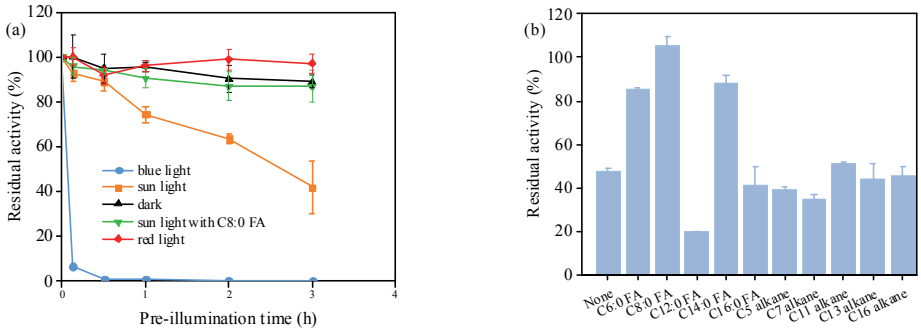

Fig. 8. Effect of illumination on the activity of *Mc*FAP-S (a) and residual activity of *Mc*FAP upon illumination in the presence of various fatty acids (b). (a) Pre-illumination conditions: blue light (400–520 nm), visible light i.e., sun light (380–780 nm), dark, red light (620–760 nm) were selected. *Mc*FAP-S pure enzyme solution (40 μmol L^{-1}_{final}) was incubated in the above light source at room temperature (25 °C) for a certain time (0, 10, 30 min, 1, 2 and 3 h). Sun light with C8:0 FA:10 mmol L^{-1}_{final} C8:0 FA. Calculate the residual enzyme activity of *Mc*FAP-S pure enzyme solution after incubation, reaction conditions: 24 μmol L^{-1} *Mc*FAP-S, 20 mmol L^{-1} *n*-octanoic acid, 15% (*v*/*v*) DMSO, 50 mmol L^{-1} Tris-HCl pH 9 of 1 mL total system in a glass vials, 30 min, 30 °C, 500 r min^{-1}, under the homemade photoenzymatic decarboxylation reaction setup (Fig. S1). (b) Pre-illumination conditions: pre-illumination 2 h, 25 °C, under sun light (380–780 nm). Reaction conditions: 20 μmol L^{-1} *Mc*FAP-S, 20 mmol L^{-1} *n*-octanoic acid, 15% (*v*/*v*) DMSO, 50 mmol L^{-1} Tris-HCl pH 9 of 1 mL total system in a glass vials, 30 min, 30 °C, 500 r min^{-1}, under the homemade photoenzymatic decarboxylation reaction setup (Fig. S1).

*Mc*FAP-S, respectively (Fig. 10(a), Figs. S8 and S9).

Next to some differences in the substrate access channel, amino acids S288, L339 and T340 as well as the region around amino acids 344-347 were identified as major differences between *Mc*FAP-S and *Cv*FAP. Docking some carboxylic acids into the active sites of both enzymes also confirmed the observed difference in substrate chain length (Figs. 10(b), (c) and Fig. S10).

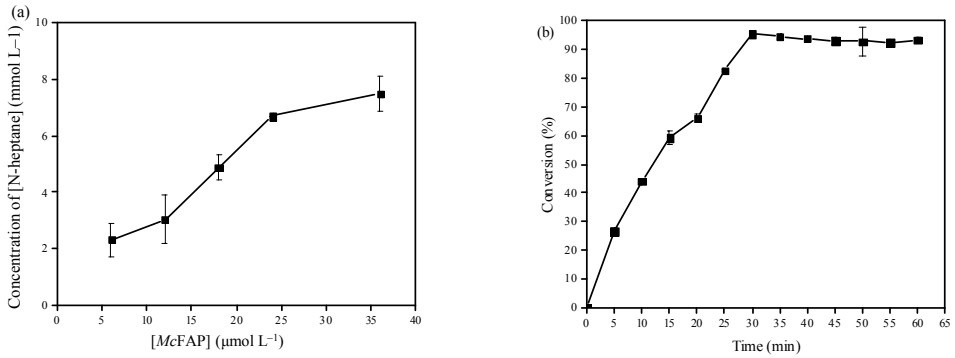

Fig. 9. Effect of enzyme concentration on the rate of the *Mc*FAP-S catalysed decarboxylation of *n*-octanoic acid (a) and time-conversion curve of purified *Mc*FAP-S catalyzing *n*-octanoic acid decarboxylation (b). General conditions: (a) 20 mmol L^{-1} *n*-octanoic acid, 15% (*v*/*v*) DMSO, 50 mmol L^{-1} Tris-HCl pH = 9.0 of 1 mL total system in a glass vials, 30 min, 30 °C, 500 r min^{-1}, under the homemade photoenzymatic decarboxylation reaction setup (Fig. S1); (b) 60 μmol L^{-1} *Mc*FAP-S, 20 mmol L^{-1} *n*-octanoic acid, 15% (*v*/*v*) DMSO, 50 mmol L^{-1} Tris-HCl pH = 9 buffer of 1 mL total system in a glass vials, 30 °C, 500 r min^{-1}, under the homemade photoenzymatic decarboxylation reaction setup (Fig. S1).

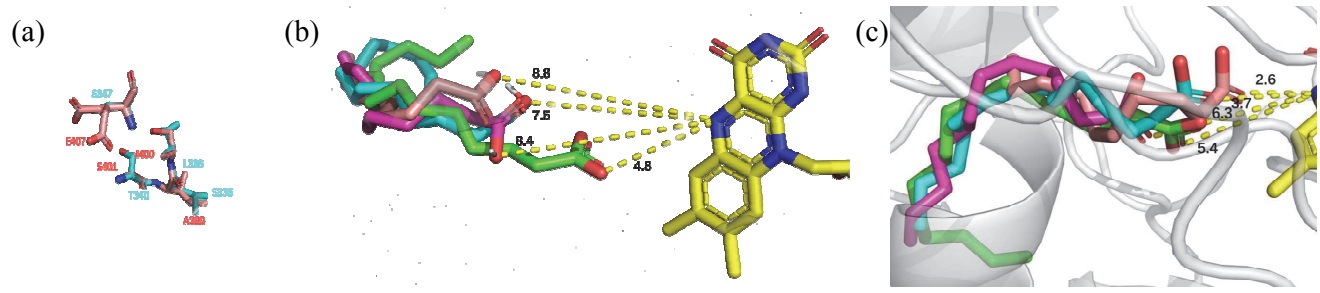

Fig. 10. Structural comparison of *Mc*FAP-S (cyan) and *Cv*FAP (rose red) (a) and molecular docking of some carboxylic acids into the active sites of *Cv*FAP (b) and *Mc*FAP-S (c). *Cv*FAP: C10:0 (pink, 8.8 Å), C12:0 (rose red, 8.4 Å), C14:0 (blue, 7.5 Å), C16:0 (green, 4.8 Å); *Mc*FAP-S: C10:0 (pink, 2.6 Å), C12:0 (rose red, 6.3 Å), C14:0 (blue, 3.7Å), C16:0 (green, 5.4 Å).

We therefore, generated some *Mc*FAP-S mutants to explore the influence of the amino acid positions 288, 339, 340 and 344–347 on the carboxylic acid preference of *Mc*FAP-S (Figs. S14–S17). While the single mutations exhibited some differences in their substrate acceptance profile, especially the triple mutant S338A/L339I/T340S exhibited a significantly decreased preference for shorter chain carboxylic acids (Fig. 11(a)).

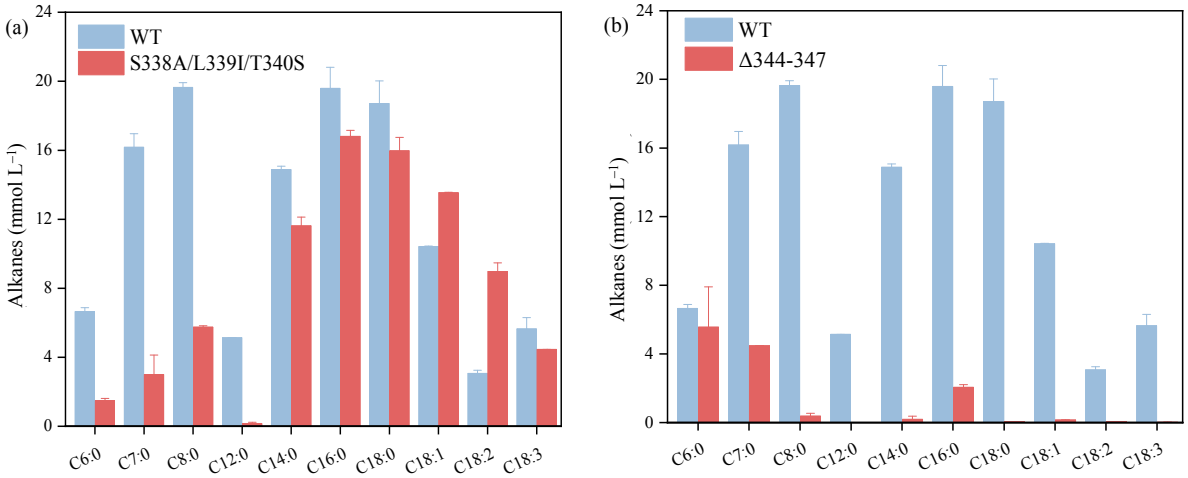

Fig. 11. Comparison of the catalytic performance of wt-*Mc*FAP-S and its triple mutant (S338A/L339I/T340S)-*Mc*FAP-S (a) and comparison of the catalytic performance of wt-*Mc*FAP-S and (Δ344–347)*Mc*FAP-S (b). Reaction conditions: (a) 40 μmol wt-*Mc*FAP-S or triple mutant (S338A/L339I/T340S)-*Mc*FAP-S, 50 mmol L^{-1} fatty acid substrate, 15% (*v*/*v*) DMSO, pH 9 buffer (50 mmol L^{-1} Tris-HCl) were mixed and under gentle magnetic stirring (500 rpm) at 30 °C in a total volume of 1 mL under the homemade photoenzymatic decarboxylation reaction setup (Fig. S1) for 1 h; (b) 40 μmol L^{-1} wt-*Mc*FAP-S or (Δ344–347)*Mc*FAP-S, 50 mmol L^{-1} fatty acid substrate, 15% (*v*/*v*) DMSO, pH = 9 buffer (50 mmol L^{-1} Tris-HCl) were mixed and under gentle magnetic stirring (500 r min^{-1}) at 30 °C in a total volume of 1 mL under the homemade photoenzymatic decarboxylation reaction setup (Fig. S1) for 1 h.

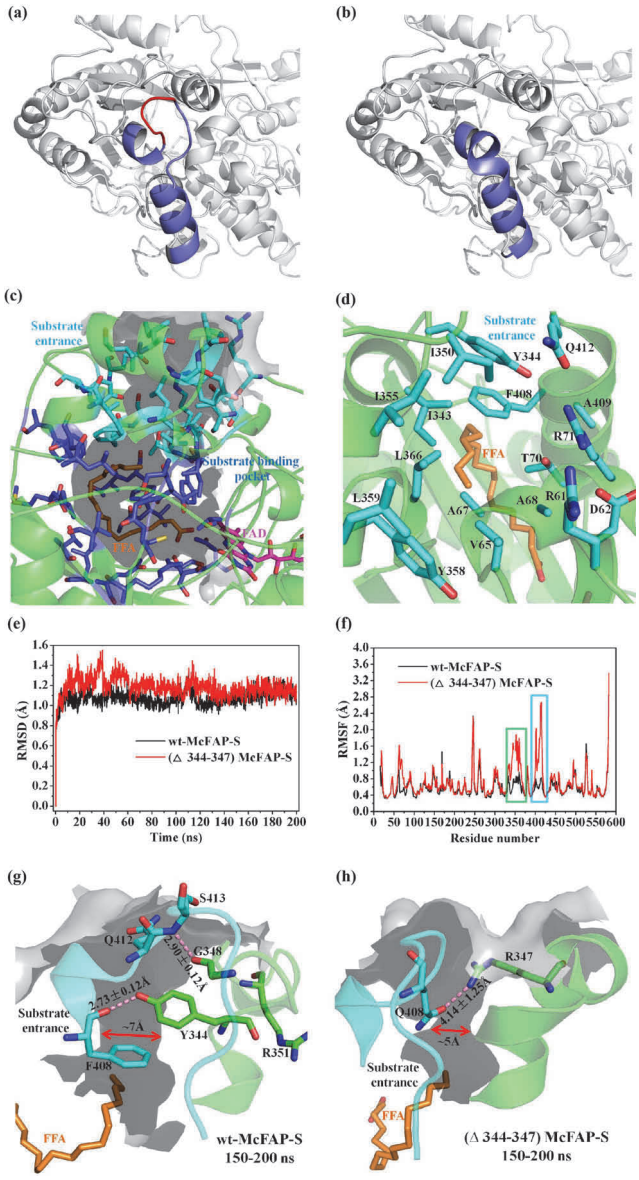

Fig. 12. Structural comparison of wt-*Mc*FAP-S and (Δ344–347) *Mc*FAP-S. (a) structural of WT wt-*Mc*FAP-S. (b) structural of WT wt-*Mc*FAP-S. (c,d) the FFA substrate tunnel of wt-*Mc*FAP-S. (e,f) The 200ns MD simulation results. (g,h) MD trajectory analysis).

Interestingly the deletion mutant Δ344–347 had almost no activity on longer chain carboxylic acids but still exhibited some activity towards hexanoic- and heptanoic acid (Fig. 11(b)).

Homology modelling of Δ344–347 indicated that the original architecture comprising two helices and one loop was transformed into a single helical region with increased rigidity (Fig. 12). This reduced flexibility may impede longer chain starting materials from entering the enzyme active site.

As shown in Fig. 12(a), in wild type model, region 339–361 formed a confirmation where two helixes were connected by a long loop. After cutting off the part close to substrate tunnel (334–337, the image of the region see Fig. 12(a)), the homologous modeling shows that the model with minimised energy is a large helix (blue part in Fig. 12(b)), which may influence the geometry of the substrate binding path. The truncated mutant loses most of the enzyme activity and retains only hexanoic acid and heptanic acid has low catalytic activity (Fig. 11).

Structural analysis showed that the FFA substrate tunnel of wt-*Mc*FAP-S can be divided into two parts, substrate entry and substrate binding pocket (Fig. 12(c), the constituent residues are shown in cyan and blue stick respectively; the specific residues of its substrate entry see Fig. 12(d)).

The 200ns MD simulation results show that the RMSD of the main chain of wt-*Mc*FAP-S and (Δ344–347) *Mc*FAP-S model (including FAD) is consistent (Fig. 12(e)), which indicates that mutation has little effect on the overall structure of wt-*Mc*FAP-S. However, the RMSF of the regions G336–S364 and D396–S416 of (Δ344–347) *Mc*FAP-S were more flexible compared to the corresponding positions of wt-*Mc*FAP-S (Fig. 12(f), the two regions were marked with green and cyan boxes, respectively). MD trajectory analysis found that Y344 and G348 formed a stable hydrogen bond with F408 and S413, respectively, in wt-*Mc*FAP-S (Fig. 12(g)), while in the corresponding position of (Δ344–347) *Mc*FAP-S, there was only a weak and unstable interaction between R347 and Q408 (Fig. 12(h)). This may be the reason why the conformational instability increases after the truncation of the surficial loop of wt-*Mc*FAP-S. Further analysis of the geometry of the substrate entry found that after the truncation of region 344–347, the rearrangement of the side chain conformation of residues in this region also led to the reduction of the size of wt-*Mc*FAP-S substrate entry (Figs. 12(g) and (h), the diameter at the narrowest part was reduced from ~7 to ~5 Å). The reduced stability and size of the substrate entry conformation reduced the catalytic activity of (Δ344–347) *Mc*FAP-S and made it difficult to bind bulky long-chain FFA.

In conclusion, the biochemical characterisation of *Mc*FAP provide some preliminary insights into the molecular origin of substrate selectivity of FAPs. The size of the substrate channel inlet and the catalytic cavity space behind the inlet are important factors affecting the substrate selectivity. These two aspects have important influence on the binding force of the channel opening to the far end of the carboxyl group of the substrate. When the binding force is low (for example *Mc*FAP), the substrate can enter the active site through the pocket entrance smoothly, which shows that the carboxyl group of the substrate is close to FAD. When this force is relatively strong, the far end of the carboxyl group of the substrate is bound to the entrance, and the substrate cannot enter the active center, which is manifested as the carboxyl group of the substrate is far from FAD. Compared to *Cv*FAP, *Mc*FAP-S has a wider channel inlet and the cavity space behind the inlet is narrower, which reduces the channel's affinity to the alkyl chains of the substrate acids and facilitates interaction with the catalytic flavin moiety.

4. Conclusions

In conclusion, we report a new member of the FAP family. *Mc*FAP show a unique chain carboxylic acids substrate selectiv-

Graphical Abstract

Chin. J. Catal., 2023, 44: 160–170 doi: 10.1016/S1872-2067(22)64173-1

A photodecarboxylase from *Micractinium conductrix* active on medium and short-chain fatty acids

Yunjian Ma, Xuanru Zhong, Bin Wu, Dongming Lan, Hao Zhang, Frank Hollmann *, Yonghua Wang *
South China University of Technology, China; Macau University of Science and Technology, China;
Delft University of Technology, The Netherlands; Guangdong Youmei Institute of Intelligent Bio-manufacturing Co., Ltd, China

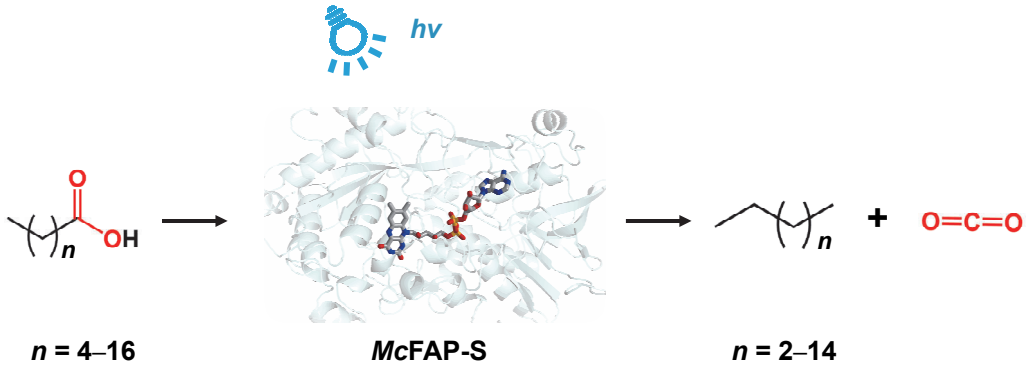

A photodecarboxylase from *Micractinium conductrix* active on medium and short-chain fatty acids shows unique chain carboxylic acids substrate selectivity compared to the well-known *Cv*FAP.

ity compared to the well-known *Cv*FAP. A structural comparison between both enzymes gives insights into the molecular basis for substrate acceptance of FAPs, which may guide future enzyme engineering efforts to generate tailored FAPs.

Author contribution statement

Yunjian Ma and Xuanru Zhong conceived, designed the study, and performed the experiments, Dongming Lan, Bin Wu and Hao Zhang analyzed the experimental data. Frank Hollmann assisted in data interpretation and manuscript formulation. Frank Hollmann and Yonghua Wang designed and directed the whole project. All the authors contributed to scientific discussion. The article was written based on contributions from all authors.

Declaration of Competing Interest

The authors declare no conflict of interest.

Electronic supporting information

Supporting information is available in the online version of this article.

References

[1] T. M. Hedison, D. J. Heyes, N. S. Scrutton, *Cur. Res. Chem. Biol.*, **2022**, 2, 100017.
[2] B. S. Chen, Y. Y. Zeng, L. Liu, L. Chen, P. Duan, R. Luque, R. Ge, W. Zhang, *Renew. Sust. Energy Rev.*, **2022**, 158, 112178.
[3] G. J. S. Dawes, E. L. Scott, J. Le Notre, J. P. M. Sanders, J. H. Bitter, *Green Chem.*, **2015**, 17, 3231–3250.
[4] D. Sorigué, B. Légeret, S. Cuiné, S. Blangy, S. Moulin, E. Billon, P. Richaud, S. Brugière, Y. Couté, D. Nurizzo, P. Müller, K. Brettel, D. Pignol, P. Arnoux, Y. Li-Beisson, G. Peltier, F. Beisson, *Science*, **2017**, 357, 903–907.
[5] Y. Wu, C. E. Paul, F. Hollmann, *ChemBioChem*, **2021**, 22, 2420–2423.
[6] J. W. Song, Y. Baeg, J. Lee, D. K. Oh, F. Hollmann, J.-B. Park, *ChemCatChem*, **2021**, 13, 4080–4086.
[7] H. T. Duong, Y. Wu, A. Sutor, B. O. Burek, F. Hollmann, J. Z. Bloh, *ChemSusChem*, **2021**, 14, 1053–1056.
[8] W. Zhang, M. Ma, M. Huijbers, G. A. Filonenko, E. A. Pidko, M. van Schie, S. de Boer, B. O. Burek, J. Bloh, W. J. H. van Berkel, P. W. A. Smith, F. Hollmann, *J. Am. Chem. Soc.*, **2019**, 141, 3116–3120.
[9] M. M. E. Huijbers, W. Zhang, F. Hollmann, *Angew. Chem. Int. Ed.*, **2018**, 57, 13648–13651.
[10] P. Santner, L. K. Szabó, S. N. Chanquia, A. H. Merrild, F. Hollmann, S. Kara, B. E. Eser, *ChemCatChem*, **2021**, 13, 4038–4046.
[11] S. Moulin, B. Legeret, S. Blangy, D. Sorigue, A. Burlacot, P. Auroy, Y. Li-Beisson, G. Peltier, F. Beisson, *Sci. Rep.*, **2019**, 9, 1–8
[12] S. Bruder, E. J. Moldenhauer, R. D. Lemke, R. Ledesma-Amaro, J. Kabisch, *Biotechnol. Biofuels*, **2019**, 12, 202.
[13] B. Lakavath, T. M. Hedison, D. J. Heyes, M. Shanmugam, M. Sakuma, R. Hoeven, V. Tilakaratna, N. S. Scrutton, *Anal. Biochem.*, **2020**, 600, 113749.
[14] D. J. Heyes, B. Lakavath, S. J. O. Hardman, M. Sakuma, T. M. Hedison, N. S. Scrutton, *ACS Catal.*, **2020**, 10, 6691–6696.
[15] M. Amer, E. Z. Wojcik, C. Sun, R. Hoeven, J. M. X. Hughes, M. Faulkner, I. S. Yunus, S. Tait, L. O. Johannissen, S. J. O. Hardman, D. J. Heyes, G.-Q. Chen, M. H. Smith, P. R. Jones, H. S. Toogood, N. S. Scrutton, *Energy Environ. Sci.*, **2020**, 13, 1818–1831.
[16] Y. Ma, X. Zhang, W. Zhang, P. Li, Y. Li, F. Hollmann, Y. Wang, *ChemPhotoChem*, **2020**, 4, 39–44.

[17] W. Zhang, J.-H. Lee, S. H. H. Younes, F. Tonin, P.-L. Hagedoorn, H. Pichler, Y. Baeg, J.-B. Park, R. Kourist, F. Hollmann, *Nat. Commun.*, **2020**, 11, 2258.
[18] H. J. Cha, S. Y. Hwang, D. S. Lee, A. R. Kumar, Y. U. Kwon, M. Voss, E. Schuiten, U. T. Bornscheuer, F. Hollmann, D. K. Oh, J. B. Park, *Angew. Chem. Int. Ed.*, **2020**, 59, 7024–7028.
[19] Q. Wu, J. Xu, Y. Hu, J. Fan, M. Arkin, D. Li, Y. Peng, W. Xu, X. Lin, *Angew. Chem. Int. Ed.*, **2019**, 58, 8474–8478.
[20] J. C. Gordon, J. B. Myers, T. Folta, V. Shoja, L. S. Heath, A. Onufriev, *Nucleic Acids Res.*, **2005**, 33, W368–W371.
[21] J. Wang, R. M. Wolf, J. W. Caldwell, P. A. Kollman, D. A. Case, *J. Comput. Chem.*, **2004**, 25, 1157–1174.
[22] G. W. T. M. J. Frisch, H. B. Schlegel, G. E. Scuseria, M. A. Robb, J. R. Cheeseman, G. Scalmani, V. Barone, G. A. Petersson, H. Nakatsuji, X. Li, M. Caricato, A. Marenich, J. Bloino, B. G. Janesko, R. Gomperts, B. Mennucci, H. P. Hratchian, J. V. Ortiz, A. F. Izmaylov, J. L. Sonnenberg, D. Williams-Young, F. Ding, F. Lipparini, F. Egidi, J. Goings, B. Peng, A. Petrone, T. Henderson, D. Ranasinghe, V. G. Zakrzewski, J. Gao, N. Rega, G. Zheng, W. Liang, M. Hada, M. Ehara, K. Toyota, R. Fukuda, J. Hasegawa, M. Ishida, T. Nakajima, Y. Honda, O. Kitao, H. Nakai, T. Vreven, K. Throssell, J. A. Montgomery, Jr., J. E. Peralta, F. Ogliaro, M. Bearpark, J. J. Heyd, E. Brothers, K. N. Kudin, V. N. Staroverov, T. Keith, R. Kobayashi, J. Normand, K. Raghavachari, A. Rendell, J. C. Burant, S. S. Iyengar, J. Tomasi, M. Cossi, J. M. Millam, M. Klene, C. Adamo, R. Cammi, J. W. Ochterski, R. L. Martin, K. Morokuma, O. Farkas, J. B. Foresman, D. J. Fox, *Gaussian 09*, *Gaussian, Inc., Wallingford,* **2016**.
[23] D. A. Case, T. A. Darden, T. E. Cheatham III, C. L. Simmerling, J. Wang, R. E. Duke, R. Luo, R. C. Walker, W. Zhang, K. M. Merz, B. Roberts, S. Hayik, A. Roitberg, G. Seabra, J. Swails, A. W. Goetz, I. Kolossváry, K. F. Wong, F. Paesani, J. Vanicek, R. M. Wolf, J. Liu, X. Wu, S. R. Brozell, T. Steinbrecher, H. Gohlke, Q. Cai, X. Ye, J. Wang, M.-J. Hsieh, G. Cui, D. R. Roe, D. H. Mathews, M. G. Seetin, R. Salomon-Ferrer, C. Sagui, V. Babin, T. Luchko, S. Gusarov, A. Kovalenko, P. A. Kollman, *University of California, San Francisco*, **2014**.
[24] W. L. Jorgensen, J. Chandrasekhar, J. D. Madura, R. W. Impey, M. L. Klein, *J. Chem. Phys.*, **1983**, 79, 926–935.
[25] W. D. Cornell, P. Cieplak, C. I. Bayly, I. R. Gould, K. M. Merz, D. M. Ferguson, D. C. Spellmeyer, T. Fox, J. W. Caldwell, P. A. Kollman, *J. Am. Chem. Soc.*, **1995**, 117, 5179–5197.
[26] V. Hornak, R. Abel, A. Okur, B. Strockbine, A. Roitberg, C. Simmerling, *Proteins-Struct. Funct. Bioinfor.,* **2006**, 65, 712–725.
[27] J. Wang, P. Cieplak, P. A. Kollman, *J. Comput. Chem.,* **2000**, 21, 1049–1074.
[28] J.-P. Ryckaert, G. Ciccotti, H. J. C. Berendsen, *J. Comput. Phys.,* **1977**, 23, 327–341.
[29] R. W. Pastor, B. R. Brooks, A. Szabo, *Mol. Phys.,* **1988**, 65, 1409–1419.
[30] S. Kumar, G. Stecher, M. Li, C. Knyaz, K. Tamura, *Mol. Biol. Evol.*, **2016**, 33, 1870–1874.
[31] D. Sorigué, K. Hadjidemetriou, S. Blangy, G. Gotthard, A. Bonvalet, N. Coquelle, P. Samire, A. Aleksandrov, L. Antonucci, A. Benachir, S. Boutet, M. Byrdin, M. Cammarata, S. Carbajo, S. Cuiné, R. B. Doak, L. Foucar, A. Gorel, M. Grünbein, E. Hartmann, R. Hienerwadel, M. Hilpert, M. Kloos, T. J. Lane, B. Légeret, P. Legrand, Y. Li-Beisson, S. L. Y. Moulin, D. Nurizzo, G. Peltier, G. Schirò, R. L. Shoeman, M. Sliwa, X. Solinas, B. Zhuang, T. R. M. Barends, J.-P. Colletier, M. Joffre, A. Royant, C. Berthomieu, M. Weik, T. Domratcheva, K. Brettel, M. H. Vos, I. Schlichting, P. Arnoux, P. Müller, F. Beisson, *Science*, **2021**, 372, eabd5687.
[32] S. L. Y. Moulin, A. Beyly-Adriano, S. Cuiné, S. Blangy, B. Légeret, M. Floriani, A. Burlacot, D. Sorigué, P.-P. Samire, Y. L. Beisson, G. Peltier, F. Beisson, *Plant Physiol.*, **2021**, 186, 1455–1472.

绿藻来源光脱羧酶*Mc*FAP的挖掘及其中短链脂肪酸选择性脱羧机制研究

马云建[a,b], 仲宣儒[a], 吴　斌[c], 蓝东明[a], 张　皓[a], Frank Hollmann[d,*], 王永华[a,e,*]

[a]华南理工大学食品科学与工程学院, 广东广州510640, 中国
[b]澳门科技大学中药质量研究国家重点实验室, 创新药物发现Neher生物物理学实验室, 澳门999078, 中国
[c]华南理工大学生物科学与工程学院, 广东广州510006, 中国
[d]代尔夫特理工大学生物技术系, 代尔夫特, 荷兰
[e]广东优酶生物制造研究院有限公司, 广东佛山528200, 中国

摘要: 利用脂肪酸脱羧制备烃类生物燃料是开发可再生能源的有效途径. 相比于传统化学法, 生物酶法具备高效、能耗低及环境友好等优势, 更具有工业应用前景. 光脱羧酶(FAP)是一类专一性强, 催化效率高, 催化过程无需额外添加昂贵辅因子, 仅需利用蓝光即可将脂肪酸转化为烷(烯)烃的光驱动酶, 在烃类生物燃料的高效可持续生物合成领域具有应用潜力. 目前已报道的有偏好催化C12-C20链长脂肪酸的光脱羧酶, 但其底物选择性机制尚未被深入探究.

本文挖掘了来源于绿藻*Micractinium conductrix*的光脱羧酶*Mc*FAP, 并开展了异源表达及制备、酶学性质表征、催化特性及底物选择性机制等研究. 利用全基因合成技术获得了来源于绿藻*Micractinium conductrix*假定的光脱羧酶基因序列*mcfap*, 同时构建了N端缺失突变体*Mc*FAP-S (缺失1-550位氨基酸). 在大肠杆菌中实现了*Mc*FAP-S的异源表达. 重组的*Mc*FAP-S对链长为6–18的饱和直链脂肪酸均有脱羧活性, 偏好中链脂肪酸, 最适底物为正辛酸(C8:0) (转化率>99%). 相同条件下, *Mc*FAP全细胞催化软脂酸(C16:0)脱羧的转化率是*Cv*FAP(来源于*Chlorella variabilis*)的1.7倍.

重组的*Mc*FAP-S催化正辛酸脱羧的最适反应温度为40 °C, 孵育6 h后残余酶活力为70.2%; 最适pH值为8.0, 孵育5 d后残余酶活力为65.4%; 对甲醇, DMSO等有机溶剂及Ni^{2+}, Ca^{2+}等金属离子具有良好的耐受性; 4 °C避光条件下储存10 d残余酶活力为76.7%. 考察了不同波长光对*Mc*FAP-S酶活力的影响, 结果表明, 红光照射3 h后*Mc*FAP-S残余酶活力为97.2%; 在可见光照射下*Mc*FAP-S与正辛酸共孵育3 h后残余酶活力> 99%. *Mc*FAP-S在30 °C, pH 9.0, 加酶量为60 μmol L^{-1}的条件下催化正辛酸脱羧, 反应30 min后转化率为95.3%.

构建了*Mc*FAP-S三维结构模型, 通过与*Cv*FAP的三维结构对比分析, 推测底物通道口大小对*Mc*FAP-S底物选择性有重要影响, 根据二者对不同链长底物结合位置的区别, 设计了突变体S338V, S338L, S338A, L339I, T340A, T340S, *Mc*FAP-S338A/L339I/T340S及Δ344–347. 结果表明, S338L仅保留催化软脂酸脱羧活力(是野生型的3.7%); L339I对正庚酸(C7:0)脱羧活力相较于野生型降低了15%, 对月桂酸(C12:0)脱羧活力增加了28%; T340S对正己酸(C6:0)脱羧活力降低了67%; S338A/L339I/T340S对正己酸脱羧活力降低了78%. 以上表明, S338, L339, T340可能是参与该酶底物选择性调控的关键位点.

综上所述, 相较已报道的*Cv*FAP催化特性, *Mc*FAP具有偏好中链脂肪酸和脱羧活性更高等优势, 提高光脱羧酶催化中链脂肪酸脱羧生成C5–C12烷烃的效率, 同时本研究初步阐明了*Mc*FAP的底物选择性机制, 可为光脱羧酶的研发及应用提供借鉴, 为阐明光脱羧酶的结构功能关系研究提供一定的基础.

关键词: 光脱羧酶; *Mc*FAP; 异源表达; 脂肪酸; 烃类生物燃料

收稿日期: 2022-07-15. 接受日期: 2022-08-31. 上网时间: 2022-12-10.

*通讯联系人. F.Hollmann@tudelft.nl (Frank Hollmann), yonghw@scut.edu.cn (王永华).

基金来源: 国家杰出青年基金(31725022); 国家自然科学基金重点项目(31930084); 中国博士后科学基金项目(2020TQ0108); 澳门青年学者计划(AM2020024).